CrossMark

Fischer–Tropsch Synthesis: XANES Spectra of Potassium in Promoted Precipitated Iron Catalysts as a Function of Time On-stream

Gary Jacobs[1,2] · Venkat Ramana Rao Pendyala[1] · Michela Martinelli[1] · Wilson D. Shafer[1] · Muthu Kumaran Gnanamani[1] · Syed Khalid[3] · Aimee MacLennan[4] · Yongfeng Hu[4] · Burtron H. Davis[1]

Abstract XANES K-edge spectra of potassium promoter in precipitated Fe catalysts were acquired following activation by carburization in CO and as a function of time on-stream during the course of a Fischer–Tropsch synthesis run for a 100Fe:2K catalyst by withdrawing catalysts, sealed in wax product, for analysis. CO-activated and end-of-run spectra of the catalyst were also obtained for a 100Fe:5K catalyst. Peaks representing electronic transitions and multiple scattering were observed and resembled reference spectra for potassium carbonate or potassium formate. The shift in the multiple scattering peak to higher energy was consistent with sintering of potassium promoter during the course of the reaction test. The catalyst, however, retained its carbidic state, as demonstrated by XANES and EXAFS spectra at the iron K-edge, suggesting that sintering of potassium did not adversely affect the carburization rate, which is important for preventing iron carbides from oxidizing. The method serves a starting point for developing better understanding of the chemical state and changes in structure occurring with alkali promoter.

Graphical Abstract
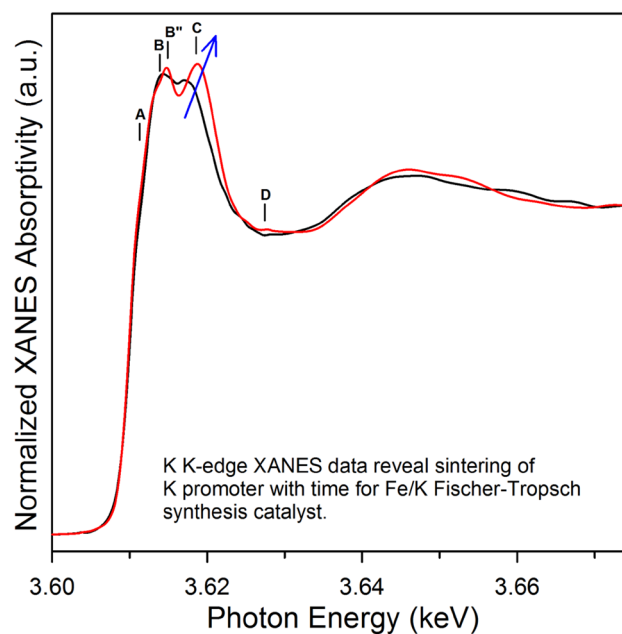
K K-edge XANES data reveal sintering of K promoter with time for Fe/K Fischer-Tropsch synthesis catalyst.

✉ Burtron H. Davis
burtron.davis@uky.edu

1 Center for Applied Energy Research, University of Kentucky, 2540 Research Park Dr., Lexington, KY 40511, USA

2 University of Texas at San Antonio, Department of Biomedical and Chemical Engineering, San Antonio, TX 78249, USA

3 NSLS, Brookhaven National Laboratories, Brookhaven Ave., Upton, NY 11973, USA

4 Canadian Light Source Inc., 44 Innovation Blvd., Saskatoon, SK S7N 2V3, Canada

1 Introduction

In Fischer–Tropsch synthesis (reactions i and ii), iron catalysts are often selected for converting syngas having low hydrogen to carbon monoxide ratio (e.g., 0.7–1.0, derived from coal or biomass) [1]. This is because iron catalysts possess intrinsic water–gas shift activity (reaction iii)

that is used to increase the H_2/CO ratio in situ in order to provide the H_2 needed to further convert CO.

(i) $(2n+1)H_2 + nCO = C_nH_{2n+2} + nH_2O$
(ii) $2nH_2 + nCO = C_nH_{2n} + nH_2O$
(iii) $CO + H_2O = H_2 + CO_2$

With pressure mounting to decrease net emissions of greenhouse gas emissions, the utilization of renewable resources, such as biomass, is receiving greater attention, making iron catalysts an attractive option. Moreover, iron catalysts have high activity for FT and may serve as a lower cost alternative to cobalt, which due to its low WGS activity, would require the process to have an additional upstream water–gas shift unit.

Promoters for iron catalysts are different from those used for cobalt. Cobalt catalysts are often promoted with a second metal (e.g., Pt, Ru, Re) [2] to facilitate the reduction of cobalt oxides—perhaps by a H_2 dissociation and spillover mechanism or a chemical effect. In contrast, in addition to structural promoters (e.g., Si), iron catalysts often contain an alkali or alkaline earth metal promoter, and often contain Cu as well. Potassium, as a result of its basic character, has been proposed to facilitate carburization during catalyst activation [3, 4], as well as influence the adsorption of the H_2 and CO reactants on the catalyst surface (e.g., promoting the dissociative adsorption of CO and preventing excessive adsorption of hydrogen) resulting in lower methane and other light gas selectivities, higher C_5+ selectivity, higher chain growth probability, and higher olefin selectivity.

Potassium has been investigated by numerous researchers over the years. Kölbel and Schneidt [5] reported that promoting precipitated iron catalysts with $0.05–0.2\%K_2CO_3$ increased surface area by up to 60%, increased the heat of reversible adsorption of CO by up to 50%, and the capacity for CO adsorption by up to 80%. Dosing with $0.6\%K_2CO_3$ was found to increase the yield of olefins from 22 to 60%. Kölbel, investigating Fe–Cu–Si catalysts, found that not only did potassium addition enhance CO chemisorption, but it also suppressed the chemisorption of hydrogen. Potassium was suggested to donate electrons to iron, promoting CO bond scission. Hydrogen, on the other hand, was proposed to donate electrons to iron such that electron donation from potassium to iron weakened the chemical bond between iron and hydrogen. Other studies have also supported the view that potassium acts to strengthen the Fe–C bond [6–8]. For example, Benziger and Madix reported that while S, O, and C tended to reduce the binding energies for CO and H, and inhibited the dissociation of CO, potassium was found to enhance the binding strengths of CO and H, and promoted the dissociation of CO. The enhanced binding energy of CO was proposed to be due to

interactions between the K 4s orbital and the CO 2π* anti-bonding orbital.

Some studies have shown that potassium increases the catalytic activity of Fischer–Tropsch synthesis and water–gas shift and/or provides benefits in terms of selectivity. For example, Bukur et al. [9] found that 0.2–1 wt% K resulted in not only significant increases in FT and WGS activity, but also increases in selectivities to olefins and heavier products, with decreases in methane and C_2-C_4 light gas selectivities. In a systematic investigation of K-promoted Fe catalysts (100Fe:0K, 100Fe:0.5K, 100Fe:1.0K, 100Fe:2.0K), a selectivity comparison at constant conversion resulted in a systematic decrease in C_1 and C_2–C_4 light gas selectivities, with systematic increases in C_5+ selectivity and chain growth probability with increasing K content [10].

In that same investigation, a detailed study using Mössbauer spectroscopy and TEM was conducted to determine the effect of potassium content on deactivation rate. The unpromoted and heavily promoted catalysts (100Fe:2K) deactivated rapidly within 200 h of time on-stream at 270 °C, 13 atm, $H_2/CO = 0.7$, and SV = 3 SL/g_{cat} h. On the other hand, moderate levels (e.g., 100Fe:0.5 K) resulted in much higher stability. Interestingly, the characterization data indicated that the unpromoted Fe catalyst deactivated by oxidization to Fe_3O_4, while the 2K promoted catalyst deactivated by the formation of more carbon-rich iron carbides or intense carbon buildup as a function of time onstream. Thus, the carburization rate during FTS should be rapid enough to prevent oxidation of active iron carbides (e.g., χ-Fe_5C_2) but slow enough to avoid excessive carbon buildup or the formation of less active iron carbides having higher C/Fe ratios.

To date, all of these studies focus solely on how K affects the state of Fe as well as catalyst performance. There has been a scarcity in literature that report on the chemical state of potassium or how the structure of potassium changes during the course of the FTS reaction. In the current contribution, soft X-rays were used to probe the K absorption edge of potassium. Samples were retrieved from the reactor as a function of time on-stream, and solidified in the solid FT wax for analysis. A comparison was made of XANES spectra of the catalysts with relevant reference compounds, and changes in XANES spectra with catalyst time on-stream were examined.

2 Experimental

2.1 Catalyst Preparation

The precipitated iron catalyst parent batch was prepared by using a ferric nitrate solution obtained by dissolving iron

(III) nitrate nonahydrate (1.17 M) in deionized water. A controlled flow of the iron nitrate mixture was added to the precipitation vessel together with a stream of ammonium hydroxide (14.8 M) that was added at a rate to maintain a pH of 9.0. The slurry was recovered using a vacuum filter and the solids were washed twice with deionized water. The final filter cake was dried for 24 h in an oven at 110 °C with flowing air. For this study, the iron catalyst base powder was then impregnated with varying amounts of aqueous potassium nitrate solution to produce a desired composition of Fe:K = 100:2.0 and 100:5.0 (atomic ratios). The K ratio between the two catalysts was confirmed by ICP to be 2.4, only slightly less than the nominal value of 2.5. Catalysts were then dried at 110 °C overnight, followed by calcination at 350 °C in flowing air for 4 h.

2.2 Catalyst Characterization

2.2.1 Surface Area and Pore Size Distribution

The measurement of BET surface area and porosity of the calcined catalysts was conducted using a Micromeritics Tri-Star system. Before performing the test, the temperature was gradually ramped to 160 °C and the sample was evacuated for 12 h to approximately 50 mTorr. The BET surface area, pore volume (single point), and average pore radius (single point) were obtained for each sample.

2.2.2 Temperature Programmed Reduction of CO

Temperature programmed reduction (TPR) of CO was conducted using a Zeton-Altamira AMI-200 unit with a thermal conductivity detector (TCD). TPR was performed using 10%CO/He at a flow rate of 30 cm³/min and catalyst samples were heated from 50 to 525 °C and held at 525 °C for 1 h. An isopropyl alcohol/dry ice trap was used to remove CO_2 from the effluent during TPR.

2.2.3 X-ray Absorption Spectroscopy

Potassium K-edge XANES spectra of catalysts and reference compounds were recorded in fluorescence mode at the Soft X-ray Micro-characterization Beamline (SXRMB) at the Canadian Light Source, Inc. Catalyst samples were removed from the continuously stirred tank reactor (CSTR) under realistic FTS conditions and sealed in the wax product for analysis to prevent exposure to air. The spectra were background subtracted and normalized with a Victoreen function and further normalized using a two-polynomial method with degree 1 for both the pre- and post-edge regions using WinXAS [11].

Iron K-edge XANES spectra (recorded at SSRL) were processed in a similar manner. For iron EXAFS data, after background removal and normalization, spectra were converted to k-space and background subtracted in k-space using a cubic spline. The spectra were truncated over the range of 2.5–10 Å⁻¹. Fe K-edge data were fitted with theoretically generated spectra from structural models assuming the presence of χ-$Fe_{2.5}C$ (Hägg carbide) and Fe_3O_4 (magnetite). Hägg carbide has a monoclinic Bravais lattice with a C 2/c space group. Lattice parameters are a = 11.504 Å, b = 4.524 Å, C = 5.012 Å, and β = 97.60°. Magnetite, on the other hand, is isometric hexoctahedral in structure with a = 8.391 Å and a space group of Fd3m. Using Atoms software [12], structural information of each contribution was converted to spatial coordinates, which were employed by FEFF [13] to determine scattering paths (Tables 1, 2). These scattering paths were inputted into FEFFIT [14] to generate theoretical χ(k), the fitting parameters of which were varied to fit the experimental data. Parameters included a global lattice expansion coefficient, α; the overall energy shift applied to each path, Δe_0; Debye–Waller factor, σ, and amplitude coefficient to account for the contribution of each phase, and particle size.

2.3 Catalyst Testing

The FTS experiments were conducted using a 1 L CSTR equipped with a magnetically driven stirrer with turbine impeller, a gas-inlet and a vapor outlet line, and a stainless steel (SS) fritted filter (2 micron) placed external to the reactor. A tube fitted with a SS-fritted filter (0.5 micron opening), extending below the liquid level of the reactor, was used to withdraw reactor wax in order to maintain a nearly constant liquid level in the reactor. Another SS diptube (1/8″ OD) extended to the bottom of the reactor and was used to withdraw aliquots of the catalyst/wax slurry from the reactor at different synthesis times. Separate mass flow controllers were used to regulate the flow of hydrogen and carbon monoxide at the desired rate. The gases were premixed in an equalization vessel before entering the reactor. Carbon monoxide was passed through a vessel containing lead oxide-alumina to remove traces of iron carbonyls. The mixed gases entered the CSTR below the stirrer, which was operated at 750 rpm. The reactor slurry temperature was maintained constant (±1 °C) by a temperature controller.

Catalyst (15 g) was added to C_{30} oil (310 g) in the CSTR to produce a slurry that contained about 5% iron oxide. The reactor temperature was then raised to 270 °C at a rate of 1 °C/min. The catalyst was activated using CO at a space velocity of 3.0 sl/h/g_{cat} at 270 °C and 175 psig for 24 h. At the end of the activation period, a sample of activated catalyst was withdrawn through the dip-tube of the CSTR. The FTS reaction was then started by adding the synthesis gas mixture to the reactor at a space velocity of 3.0 sl/h/

Table 1 Path parameters generated by FEFF (single scattering) for Hägg carbide

Hägg carbide	Atom	Interaction	#Degeneracies	Distance (Å)
	Fe2	Fe–C	1.0	1.9309
	Fe1	Fe–C	1.0	1.9433
	Fe1	Fe–C	1.0	1.9766
	Fe2	Fe–C	1.0	1.9921
	Fe3	Fe–C	2.0	2.0022
	Fe3	Fe–C	2.0	2.0388
	Fe2	Fe–C	1.0	2.3475
	Fe3	Fe–Fe	2.0	2.3616
	Fe2	Fe–Fe	1.0	2.3616
	Fe1	Fe–C	1.0	2.4964
	Fe1	Fe–Fe	1.0	2.4958
	Fe1	Fe–Fe	1.0	2.4965
	Fe3	Fe–Fe	2.0	2.4965
	Fe1	Fe–Fe	1.0	2.5415
	Fe2	Fe–Fe	2.0	2.5502
	Fe3	Fe–Fe	2.0	2.5762
	Fe1	Fe–Fe	1.0	2.5901
	Fe3	Fe–Fe	2.0	2.5901
	Fe2	Fe–Fe	2.0	2.6010
	Fe2	Fe–Fe	1.0	2.6170
	Fe1	Fe–Fe	2.0	2.6378
	Fe1	Fe–Fe	1.0	2.6428
	Fe2	Fe–Fe	1.0	2.6428
	Fe1	Fe–Fe	1.0	2.6463
	Fe2	Fe–Fe	1.0	2.6463
	Fe1	Fe–Fe	1.0	2.6737
	Fe2	Fe–Fe	1.0	2.6737
	Fe1	Fe–Fe	1.0	2.6937
	Fe3	Fe–Fe	2.0	2.6937
	Fe1	Fe–Fe	1.0	2.6988
	Fe2	Fe–Fe	1.0	2.6988
	Fe1	Fe–Fe	1.0	2.7788
	Fe2	Fe–Fe	1.0	2.7788
	Fe1	Fe–C	1.0	2.8702
	Fe1	Fe–C	1.0	3.4258
	Fe2	Fe–Fe	1.0	3.4642
	Fe3	Fe–Fe	2.0	3.4642
	Fe2	Fe–C	1.0	3.4887

Table 2 Path parameters generated by FEFF (single scattering) for magnetite

Magnetite	Atom	Interaction	#Degeneracies	Distance (Å)
	Fe1	Fe–O	1.0	1.8861
	Fe2	Fe–O	1.0	2.0602
	Fe2	Fe–Fe	1.0	2.9684
	Fe1	Fe–Fe	1.0	3.4807
	Fe2	Fe–Fe	2.0	3.4807
	Fe1	Fe–O	2.0	3.4933

the oil and the wax fractions were mixed prior to GC analysis.

3 Results and Discussion

The BET surface area and pore size distribution results of un-promoted and various potassium promoted iron catalysts are shown in Table 3. If Fe_2O_3 is the primary contributor to surface area, addition of 2 and 5 K should lead to decreases in surface area to about 42.7 and 41.9 m^2/g, respectively. However, more significant decreases were observed, to 29.0 and 31.2 m^2/g, respectively. At the same time, increases in pore diameter were observed by 42 and 31% (single point data), suggesting that potassium addition caused some pore blocking, especially of narrower pores.
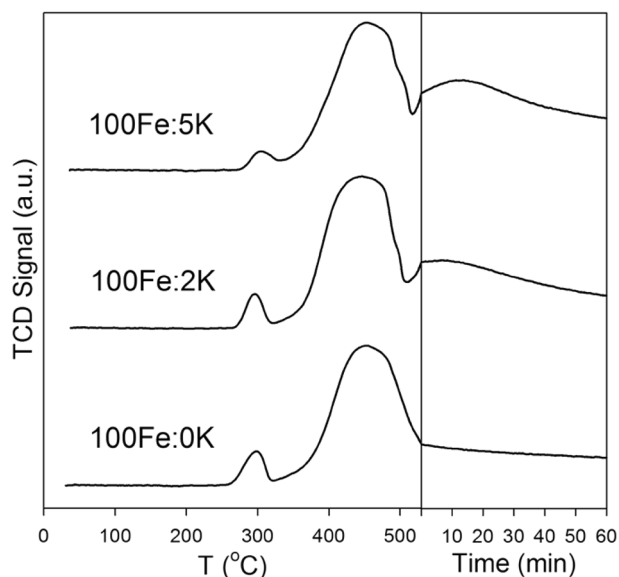
The CO TPR profiles of un-promoted and various potassium promoted iron catalysts are shown in Fig. 1. Based on TPR-XANES/EXAFS results [3], iron activation in CO proceeds in a series of steps, including: (1) reduction of Fe_2O_3 to Fe_3O_4; (2) further reduction of Fe_3O_4 to a defect-laden form resembling FeO; and (3) carburization of FeO to Fe_xC_y. The first peak in the profile, centered at close to 300 °C, is likely that of step (1), while the remaining oxide reduction steps occur in the higher temperature broad asymmetric peak. Carburization also likely begins in the asymmetric peak and continues at higher temperature and during the hold step. Based on the peak intensities during the hold procedure, CO uptake during carburization/carbon formation is more significant with addition of potassium, and as a function of potassium loading.

The effect of potassium promoter loading on CO conversion versus time-on-stream for the iron catalysts is shown in Fig. 2. At similar activation and reaction conditions (temperature, pressure and GHSV) but varying the potassium loading (2 and 5 K), high initial CO conversions (~80%) were observed for both catalysts. The activity of the catalysts gradually decreased with time-on-stream. Both catalysts exhibited similar deactivation trends. The effect of potassium promoter loading was investigated in our previous studies [10, 15], and a similar deactivation
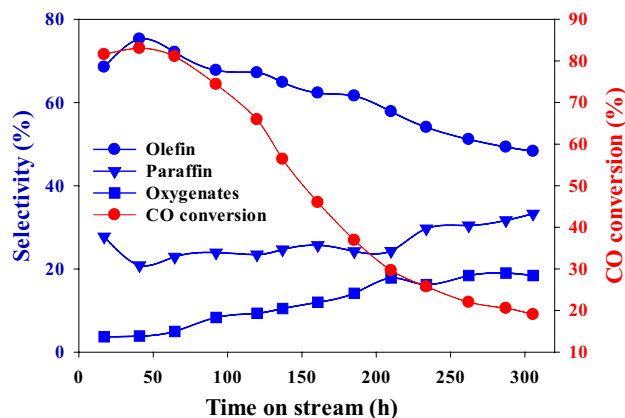
g_{cat} and a H_2/CO ratio of 0.7. The conversions of CO and H_2 were obtained by gas-chromatography analysis (micro-GC equipped with thermal conductivity detectors) of the reactor effluent. The reaction products were collected in three traps maintained at different temperatures: a hot trap (200 °C), a warm trap (100 °C) and a cold trap (0 °C). The products were separated into different fractions (rewax, wax, oil and aqueous phase) for quantification. However,

Table 3 BET surface area and porosity measurements of un-promoted and potassium promoted iron catalysts

Catalyst	BET SA (m^2/g)	Single point pore volume (cm^3/g)	BJH adsorption average pore volume (cm^3/g)	BJH desorption average pore volume (cm^3/g)	Single point pore diameter (nm)	BJH adsorption average pore diameter (nm)	BJH desorption average pore diameter (nm)
100Fe	43.2	0.203	0.209	0.209	18.8	16.4	15.0
100Fe:2K	29.0	0.194	0.199	0.199	26.7	24.0	21.0
100Fe:5K	31.2	0.193	0.192	0.194	24.7	25.0	18.6

Fig. 1 CO TPR profiles of 100Fe:0K, 100Fe:2K, and 100Fe:5K catalysts
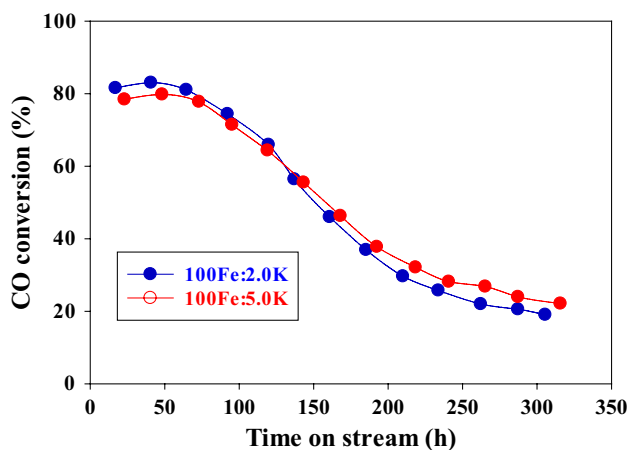
Fig. 2 CO conversion against time on stream for various potassium loaded iron catalysts

Fig. 3 CO conversion and product selectivities against time on stream of 100Fe:2.0K catalyst

trend was observed for the 100Fe:2.0K catalyst. The deactivation of these catalysts was explained by the results of Mössbauer spectroscopy and TEM techniques. The effect of deactivation on product selectivities for the 100Fe:2.0K catalyst is presented in Fig. 3. With decreasing CO conversion or with time, olefin selectivity decreased and the corresponding paraffin and oxygenate selectivities increased. The 100Fe:5.0K catalyst also exhibited similar product selectivities as compared to the 100Fe:2.0K catalyst (not shown for the sake of brevity). The oxygenate selectivity, and especially the aldehydes selectivity, was found to increase with time (i.e., decreasing CO conversion). Changes in product selectivities with time may be due to the formation of a carbon layer on the surface of the catalyst. The effect of potassium promoter versus time on hydrocarbon selectivity of 100Fe:2.0K catalyst is shown in Fig. 4. There were no significant changes observed regarding hydrocarbon selectivity (methane, C_2-C_4 and C_5+) of the catalyst either with time or CO conversion. However, the carbon dioxide selectivity decreased slightly with time. Generally, for cobalt and ruthenium based catalysts, the selectivity to lower hydrocarbons (C_1-C_4) decreases and that of the higher hydrocarbon selectivity (C_5+) increases with increasing CO conversion, whereas for an iron catalyst, the product selectivity remains more or less constant at conversions less than 70% for potassium promoted iron catalysts [16].

XANES spectra at the potassium K-edge for catalysts retrieved from the CSTR as a function of time on-stream is
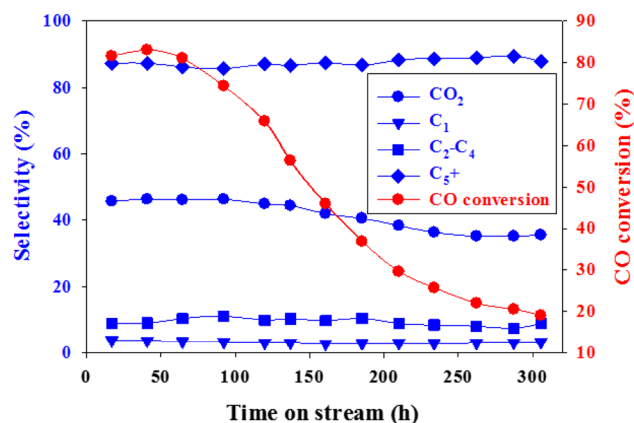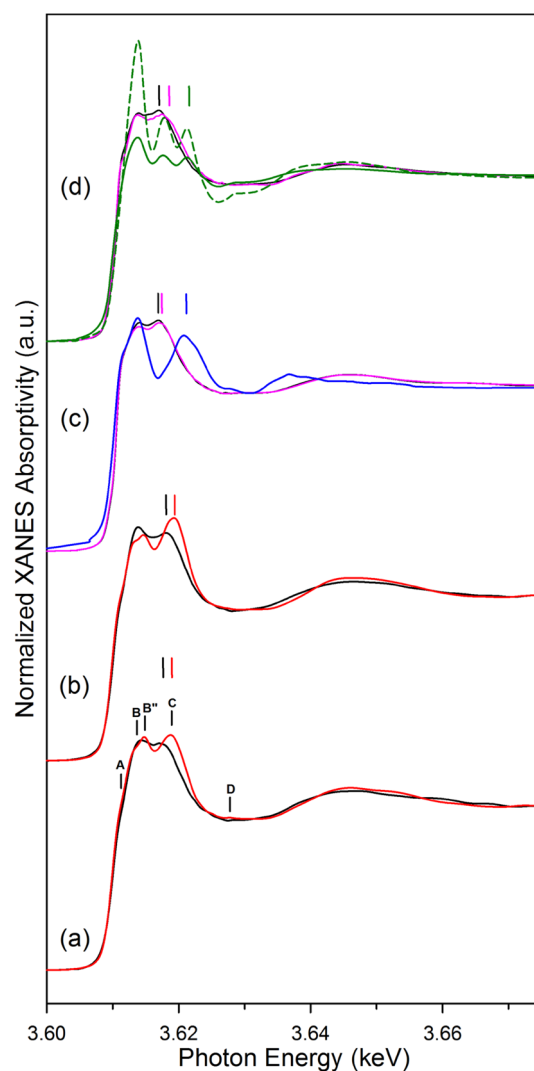
Fig. 4 Hydrocarbon and CO_2 selectivity against time on stream for a 100Fe:2.0K catalyst
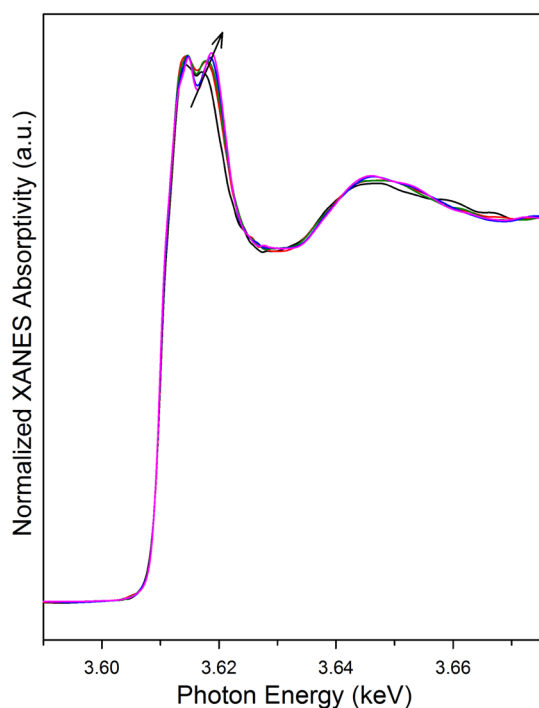
Fig. 5 Normalized K K-edge XANES spectra of the 100Fe:2K catalyst (*black*) following activation in CO at 425 °C for 6 h and, moving along the trajectory of the *arrow*, after running Fischer–Tropsch synthesis for (*red*) 24 h, (*green*) 48 h, (*blue*) 95 h, and (*pink*) 165 h

Fig. 6 Normalized K K-edge XANES spectra of *a* 100Fe:2K and *b* 100Fe:5K catalysts (*black*) after activation and (*red*) following the Fischer–Tropsch synthesis reaction test; *c* (*black*) 0.97% K_2CO_3/SiO_2, (*pink*) 2.38% K_2CO_3/SiO_2, and (*blue*) bulk K_2CO_3; and *d* (*black*) 0.97% $KHCO_2$/SiO_2, (*pink*) 2.38% $KHCO_2$/SiO_2, and (*green*) bulk $KHCO_2$

reported in Fig. 5. Within 20 eV of the edge jump, the near edge region consists primarily of a lower energy asymmetric peak with two low energy shoulders and a higher energy peak. Interestingly, with increases in time on-stream, the higher energy peak systematically increases in intensity and shifts to higher energy.

Potassium K-edge absorption spectra of numerous potassium compounds were extensively investigated by Sugiura and Muramatsu [17]. However, somewhat surprisingly, very little has been published on the potassium K-edge spectra of alkali doped catalysts. The authors examined families of potassium compounds and observed similarities (as well as some differences) in spectral features within each family. In reference to the current work, a similar splitting of peaks was found to occur in the family of compounds K_2SO_4, K_2CrO_4, and K_2MnO_4 investigated by Sugiura and Muramatsu [17]. Within that family, the authors assigned the low energy peak to electronic transitions (i.e., their Peak A pre-edge shoulder was assigned to 1*s* to 3*d*, while the main Peak B was assigned to the 1*s* to 4*p* transition) and the higher energy peak to a continuum state (i.e., multiple scattering).

Table 4 K-K edge XANES peak positions for potassium formate on SiO$_2$ and in bulk form

Notation	0.97% KHCO$_2$ on SiO$_2$	0.97% KHCO$_2$ on SiO$_2$	2.38% KHCO$_2$ on SiO$_2$	2.38% KHCO$_2$ on SiO$_2$	KHCO$_2$ bulk	KHCO$_2$ bulk
A	3.607–3.612	Shoulder	3.607–3.612	Shoulder	3.607–3.612	Shoulder
B	3.612–3.615	3.6140 s	3.612–3.615	3.6138 s	3.612–3.616	3.6138 s
B′	3.615–3.616	3.6155 w	3.615–3.616	Shoulder		
C	3.616–3.626	**3.6170 s**	3.616–3.617	Shoulder	3.616–3.620	3.6177 s
C′			3.617–3.618	**3.6175 s**	3.620–3.624	**3.6212 s**
C″			3.618–3.626	Shoulder	3.624–3.626	Shoulder
D	3.626–3.629	3.6267 w	3.626–3.628	3.6267 w	3.626–3.631	3.6294 w
E	3.629–3.635	Shoulder	3.628–3.634	3.6314 w	3.631–3.634	Shoulder
F	3.635–3.642	Shoulder	3.634–3.640	Shoulder	3.634–3.642	Shoulder
G						
H	3.642–3.650	3.6453 s	3.640–3.647	3.6445 s	3.642–3.649	3.6454 s
I	3.650–3.656	Shoulder	3.647–3.656	Shoulder	3.649–3.656	Shoulder
Notation	0.97% K$_2$CO$_3$ on SiO$_2$	0.97% K$_2$CO$_3$ on SiO$_2$	2.38% K$_2$CO$_3$ on SiO$_2$	2.38% K$_2$CO$_3$ on SiO$_2$	K$_2$CO$_3$ bulk	K$_2$CO$_3$ bulk
A	3.607–3.612	Shoulder	3.607–3.612	Shoulder	3.607–3.612	Shoulder
B	3.612–3.613	Shoulder	3.612–3.614	3.6139 s	3.612–3.617	3.6138 s
B′	3.613–3.615	3.6140 s	3.614–3.615	Shoulder		
C	3.615–3.616	Shoulder	3.615–3.616	Shoulder	3.617–3.619	Shoulder
C′	3.616–3.618	**3.6170 s**	3.617–3.619	**3.6174 s**	3.620–3.622	**3.6208 s**
C″	3.618–3.625	Shoulder	3.618–3.627	Shoulder	3.624–3.626	Shoulder
D	3.625–3.628	Shoulder	3.627–3.629	Shoulder	3.626–3.631	3.6273 w
E	3.628–3.634	3.6310 w	3.629–3.634	3.6314 w	3.631–3.635	Shoulder
F	3.634–3.640	Shoulder	3.634–3.640	Shoulder	3.635–3.638	3.6368 s
G					3.638–3.643	Shoulder
H	3.640–3.653	3.6454 s	3.640–3.647	3.6445 s	3.643–3.649	3.6451 w
I	3.653–3.658	Shoulder	3.647–3.653	Shoulder	3.649–3.653	3.6513 w

Table 5 K-K edge XANES peak positions for (black) CO-activated and (red) used catalysts after Fischer–Tropsch synthesis, including (a) 100Fe:2K and (b) 100Fe:5K

Notation	(a) Black	(a) Black	(a) Red	(a) Red	(b) Black	(b) Black	(b) Red	(b) Red
A	3.607–3.612	Shoulder	3.607–3.612	Shoulder	3.607–3.612	Shoulder	3.607–3.612	Shoulder
B	3.612–3.615	3.6143 s	3.612–3.614	Shoulder	3.612–3.615	3.6137 s	3.612–3.614	3.6134
B'	3.615–3.616	Shoulder	3.614–3.616	3.6148 s	3.615–3.616	Shoulder	3.614–3.616	3.6146 s
C	3.616–3.617	Shoulder	3.616–3.617	Shoulder	3.616–3.617	Shoulder	3.616–3.617	Shoulder
C′	3.617–3.619	**3.6175 s**	3.617–3.627	**3.6188 s**	3.617–3.619	**3.6180 s**	3.617–3.628	**3.6194 s**
C″	3.619–3.626	Shoulder			3.619–3.626	Shoulder		
D	3.626–3.629	Shoulder	3.627–3.630	3.6279 w	3.626–3.628	Shoulder	3.628–3.632	3.6311 w
E	3.629–3.634	Shoulder	3.630–3.634	Shoulder	3.628–3.634	Shoulder	3.632–3.634	Shoulder
F	3.634–3.640	Shoulder	3.634–3.639	Shoulder	3.634–3.638	Shoulder	3.634–3.639	Shoulder
G								
H	3.642–3.652	3.6475 s	3.639–3.649	3.6464 s	3.638–3.650	3.6475 s	3.639–3.652	3.6462 s
I	3.652–3.656	Shoulder	3.649–3.656	Shoulder	3.652–3.655	Shoulder	3.652–3.659	Shoulder

Related to the potassium K-edge spectra of the K/Fe catalysts obtained in this work, the assignments by Sugiura and Muramatsu [17] make logical sense, as the peak for electronic transitions should remain stationary while the multiple scattering peak should be sensitive to changes in the local atomic environment. It has been speculated that

the K compound in Fe-based FTS catalysts may be K_2CO_3 or KHCOO, or a related species. To test the idea that the second peak is due to multiple scattering, reference compounds were prepared of K_2CO_3 and KHCOO supported on silica and for each compound two different concentrations were used; in addition, spectra of the bulk reference compounds were also analyzed. These reference spectra are provided as (c) and (d) in Fig. 6. The results indicate that increasing the concentration of the reference compound supported on silica or using the bulk reference compound did not significantly alter the energy position of the first peak; this indicates the first peak is likely due to electronic transitions. However, increasing the concentration of the dispersed reference compound on silica, or moving from supported reference compound to the bulk reference compound, the second peak moves systematically to higher energy; this is consistent with the assignment by Sugiura and Muramatsu [17] that the peak is a continuum multiple scattering feature. In the case of potassium formate, the peak assigned to multiple scattering splits into two peaks in moving from supported to bulk reference compound, while in the case of potassium carbonate, a similar change occurs; however, the bulk reference peak for multiple scattering exhibits asymmetric character suggesting the presence of two contributions. Note that in Fig. 6d, due to the effect of self-absorption on XANES intensity for the potassium formate reference compound in fluorescence mode, a second spectrum was taken using a TEY detector (dashed line). As shown in Table 4, Peak C (bold) of $KHCO_2$ moves from 3.6170 to 3.6175 to 3.6212 keV in moving from $0.97\%KHCO_2/SiO_2$ to $2.38\%KHCO_2/SiO_2$ and then to the bulk HCO_2 compound. Likewise, Peak C (bold) of K_2CO_3 moves from 3.6170 to 3.6174 to 3.6208 keV in moving from $0.97\%K_2CO_3$ to $2.38\%K_2CO_3$ and further to the bulk K_2CO_3 compound.

Spectra for the CO-activated catalyst and the catalyst following the FTS reaction are also shown. Peaks due to electronic transitions are listed as A, B, and B′, consistent with the notation of Sugiura and Muramatsu [16]. Peak C was found to move to higher energy for both the 2 and 5 K promoted catalysts following FTS in comparison with the freshly carburized catalyst. Figure 5 emphasizes that the change in the position of Peak C (bold) occurs systematically as a function of time on-stream during the FTS reaction test. As shown in Table 5, Peak C moves from 3.6175 to 3.6188 keV for the 100Fe:2K catalyst and from 3.6180 to 3.6194 keV for the 100Fe:5K catalyst. These changes are consistent with the view of Sugiura and Muramatsu that Peak C is a continuum peak and that the local environment is changing to one of increased size/ordering with time on-stream. Also, the fact that Peak C in the spectrum of the CO-activated 5K catalyst is located at a higher energy (3.6180 keV) than that of the 2K catalyst (3.6175 keV)
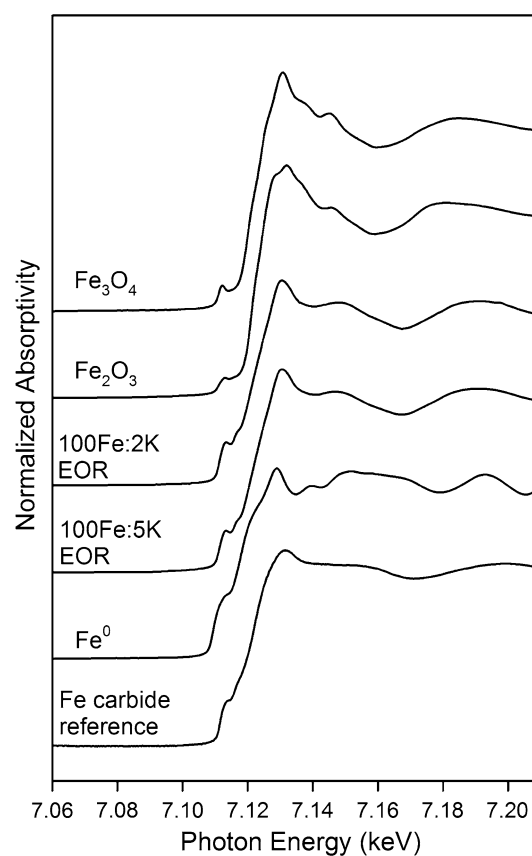
Fig. 7 Normalized XANES spectra at the K-edge of Fe for reference compounds and end-of-run (EOR) 100Fe:5K and 100Fe:2K catalysts. Note that the Fe carbide reference was following a CO-TPR/XANES experiment for a Fe:1.5K catalyst (details provided elsewhere [3])

lends further support to the view that Peak C is a multiple scattering peak whose energy moves to higher values with increased size/ordering.

These results reveal three important points: (1) the catalyst contains potassium in a well-dispersed state that does not match well that of bulk reference compounds; (2) the potassium compound located on the iron catalyst surface has similar characteristics to either potassium carbonate or potassium formate, and is likely a related compound; and (3) with time on-stream, the results strongly suggest that sintering of this surface potassium compound occurs with time, as the shift in energy position of Peak C, assigned to multiple scattering, is consistent with increasing size and crystalline order.

Sintering of potassium may be problematic for two reasons. First of all, sintering of potassium may exacerbate pore blocking, especially if there is excessive carbon being formed (e.g., the case of high potassium promoter loading [10]). Secondly, sintering removes surface potassium that otherwise promotes CO scission occurring on the Fe carbide surface. In the case of the un-promoted catalyst,
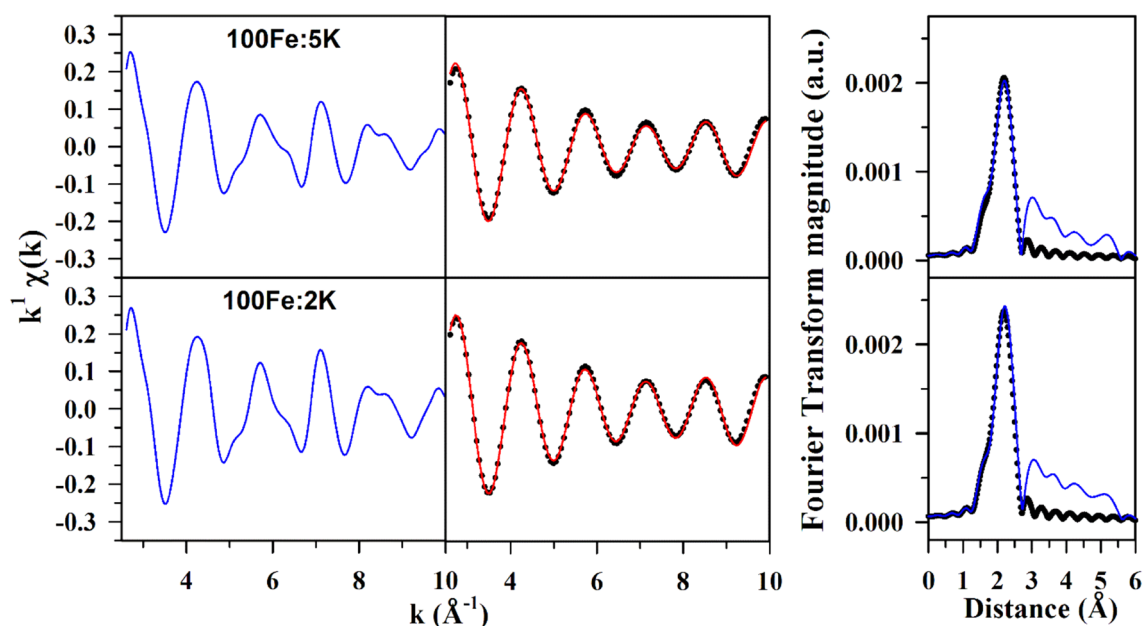
Fig. 8 EXAFS spectra at the K-edge of Fe for end-of-run 100Fe:5K and 100Fe:2K catalysts, including (*left*) raw $\chi(k)$ versus k spectra; (*middle*) (*red*) filtered $\chi(k)$ versus k and (*filled circles*) result of the

EXAFS fitting; and (*right*) (*blue*) raw k^1-weighted Fourier transform magnitude and (*filled circles*) result of the EXAFS fitting

deactivation by oxidation was found to occur [10]. Thus, there is the possibility, and especially in the case of low alkali loading, that sintering may remove a critical amount of promoter from the surface that is required to stabilize iron in a carburized state that is needed for conducting both the FTS and WGS reactions. However, although we attempted to investigate catalysts having low potassium content, the spectra were found to be too noisy to draw any conclusion.

In the current context, where high promoter loadings are utilized, loss of carbide by oxidation was not a key issue associated with deactivation. Figure 7 shows Fe K-edge XANES spectra of catalysts and reference compounds; the end-of-run (listed as EOR) catalysts display the characteristic line shape of Fe carbide consistent with a form close to

that of χ-Fe_5C_2. Figure 8 and Table 6 indicate that excellent fittings of the spectra with a Hägg carbide model could be obtained without a significant contribution from the oxide. In Mössbauer spectroscopy, the carbide identified in the EOR 2K catalyst was $Fe_{2.2}C$ and residual Fe_3O_4 was just 7%; thus, it is evident that while EXAFS provides useful supporting information, it should probably not be used to distinguish between closely related carbides.

4 Conclusions

For the first time, the K-edge of potassium was examined by XANES for investigating the changes occurring in the spectra of potassium promoter for an iron catalyst during the FTS reaction. CO-activated and end-of-run spectra for 100Fe:2K and 100Fe:5K catalysts presented peaks corresponding to electronic transitions and multiple scattering continuum states. The shift in the peak tentatively assigned to multiple scattering to higher energy was consistent with sintering of potassium promoter during the course of the reaction test. The spectra resembled that of dispersed potassium carbonate or potassium formate, although a related compound is also possible. The end-of-run catalyst retained its iron carbidic state, as demonstrated by XANES and EXAFS spectra at the iron K-edge; thus, removal of potassium due to sintering did not lead to deactivation by oxidation. However, sintering of potassium may exacerbate a deactivation mechanism involving pore blocking

Table 6 Results of EXAFS fittings for end-of-run catalyst considers the presence of Hägg carbide

Catalyst	α	A	σ^2 (Å^2)	e_0 (eV)	r-factor
100Fe:2K	0.022 (0.003)	0.73 (0.036)	0.0073 (0.0007)	6.79 (0.75)	0.0023
100Fe:5K		0.85 (0.041)		−7.63 (0.87)	

Fitting intervals: 2.5 Å^{-1} < k < 10.0 Å^{-1}; 1.5 Å < R < 2.5 Å. Note that S_0^2 was fixed at 0.9. Global parameters (i.e., over all samples) were used for the energy shift (e_0), the isotropic lattice expansion (α) and Debye–Waller factor (σ^2) parameters for Hägg carbide. Local parameters (i.e., for each sample) were used for amplitude function multipliers (A) of each catalyst

by excessive carbon formation at high K loading. The 100Fe:2K catalyst was previously found to produce excessive carbon in Mössbauer spectroscopy and TEM studies. Based on the CO TPR results and similar deactivation profile, the 100Fe:5K catalyst appears to have the same stability issue, which may be compounded by potassium sintering.

References

1. Keyvanloo K, Mardkhe MK, Alam TM, Bartholomew CH, Woodfield BF, Hecker WC (2014) ACS Catal 4:1071
2. Jacobs G, Ji Y, Davis BH, Cronauer DC, Kropf AJ, Marshall CL (2007) Appl Catal A 333:177
3. Ribeiro MC, Jacobs G, Davis BH, Cronauer DC, Kropf AJ, Marshall CL (2010) J Phys Chem C 114:7895
4. Li S, Li A, Krishnamoorthy A, Iglesia E (2001) Catal Lett 77:197
5. Kölbel H, Schneidt D (1977) Erdol Kohle Erdgas P 30:139
6. Dry ME, Shingles T, Boshoff L, Oosthuizen GJ (1969) J Catal 15:190
7. Benziger J, Madix R (1980) Surf Sci 94:119
8. Arakawa H, Bell AT (1983) Ind Eng Chem Proc Des Dev 22:97
9. Bukur DB, Mukesh DS, Patal A (1990) Ind Eng Chem Res 29:194
10. Pendyala VRR, Graham UM, Jacobs G, Hamdeh HH, Davis BH (2014) Catal Lett 144:1704
11. Ressler T (1998) J Synchrotron Rad 8:118
12. Ravel B (2001) J Synchrotron Rad 8:314
13. Rehr JJ, Albers RC (2000) Rev Mod Phys 72:621
14. Newville M, Ravel B, Haskel D, Stern EA, Yacoby Y (1995) Phys B 208–209:154
15. Pendyala VRR, Graham UM, Jacobs G, Hamdeh HH, Davis BH (2014) ChemCatChem 6:1952
16. Yang J, Ma W, Chen D, Holmen A, Davis BH (2014) Appl Catal A 470:250
17. Sugiura C, Muramatsu S (1985) Phys Stat Solidi B 132:K111